Templated Growth of Alumina-Based Fibers through the Use of Anthracenic Organogelators

M. Llusar,[†,‡] L. Pidol,[†] C. Roux,[†] Jean L. Pozzo,[§] and C. Sanchez*[,†]

Laboratoire de Chimie de la Matière Condensée, UMR CNRS 7475, Université Pierre et Marie Curie, F-75252 Paris Cedex 05, France, Departament de Química Inorgànica i Orgànica, Universitat jaume I, 12071 Castelló, Spain, and Photochimie Organique, UMR 5802, Université de Bordeaux I, F-33405, France

Received June 28, 2002. Revised Manuscript Received September 20, 2002

DDOA (2,3-bis(*n*-decyloxy)anthracene) has been successfully employed as a template to direct the growth of high-surface alumina-based fibers exhibiting bimodal porosity. Hybrid gels were obtained after thermal aging (at 40 °C) of an aqueous ethanol solution of $AlCl_3$ entrapped by a previously formed DDOA organogel. SEM characterization showed that the hybrids were constituted by submicronic fibers (200−500 nm) aggregated into fibrous bundles (1−2 μm thick), and evidenced an important effect of pH conditions on fibers thickness and on fibers aggregation (intertwined or highly co-aligned). By calcining at 350 °C, the organic imprint was satisfactorily removed (confirmed by FTIR, EDAX, and chemical analyses) without disruption of the fibrous assemblies, leading to high surface (150−300 m^2/g) alumina-based fibrous materials with an anisotropic porosity at the meso- (around 3−10 nm) and macroscales (confirmed by nitrogen sorption measurements and by TEM characterization). Very interestingly, the fibrous morphology was highly preserved after calcination at 800 °C and crystallization of transition aluminas and α-Al_2O_3.

1. Introduction

Apart from the high-temperature stable oxide α-Al_2O_3 (corundum) and from aluminum hydroxides $Al(OH)_3$ and oxyhydroxides AlO(OH), aluminas also exist as a large variety of metastable variants known as transition aluminas.[1−3] Among these transition aluminas, partially amorphous or crystalline γ-Al_2O_3 (the first member of the series resulting from dehydration of boehmite: AlO(OH) → γ-Al_2O_3 → δ-Al_2O_3 → θ-Al_2O_3 → α-Al_2O_3)[4−6] is an extremely important technological material, owing to its widespread use as sorbent[7] or as high surface-area support material for automotive catalytic converters[8] and for other types of catalysts, such as those employed in petroleum refining[9] and in the production of bulk and fine chemicals.[10] However, the physical properties and potential applications of a given material do not depend only on its chemical composition and structure but also on its texture and shape.

Indeed, materials chemists possess nowadays a set of efficient tools at hand, being able to smartly choose the texturing agents (surfactants, block copolymers, dendrimers, etc.), the starting mineral precursors (inorganic salts, metal alkoxides, NanoBuildingBlocks, etc.), and the reaction media (solvents, water contents, pH, complexing agents, aging conditions, etc.) to attempt a high control on the compatibility of the mineral and organic components, and the self-assembly processes at hybrid interfaces.[11] More recently, organogelalors being able to reversibly form fibrous networks, with well-defined geometry and shape, have been used to shape and texture inorganic materials such as silica and titania based materials.[12−20]

* To whom correspondence should be addressed. Phone: 33 1 44275534. Fax: 33 1 44274769. E-mail: clems@ccr.jussieu.fr.
† Laboratoire de Chimie de la Matière Condensée.
‡ Departament de Química Inorgànica i Orgànica.
§ Photochimie Organique.

(1) (a) Euzen, P.; Krokidis, X.; Raybaud, P.; Toulhoat, H.; Le Loarer, J. L.; Jolivet, J. P.; Froidefond, C. In *Alumina, Handbook of Porous Materials*; Schueth, F., Sing, K., Weitkamp, J. Eds.; Wiley-VCH Verlag GmbH: Weinheim, 2002, 1591−1676. (b) Wefers, K. *Alumina Chemicals: Science And Technology Handbook;* Hart L. D., Ed.; The American Ceramic Society: Westerville, OH, 1990; pp 13−22.
(2) Misra, C. *Industrial Alumina Chemicals*; ACS Monograph 184; American Chemical Society: Washington, DC, 1986.
(3) Gitzen, W. H. *Alumina as a Ceramic Material*; The American Ceramic Society: Coumbus, OH, 1970.
(4) Levin, I.; Brandon, D. *J. Am. Ceram. Soc.* **1998**, *81*, 1995.
(5) Husson, E.; Reppelin, Y., *Eur. J. Solid State Inorg. Chem.* **1996**, *33*, 1223.
(6) Krokidis, X.; Raybaud, P.; Gobichon, A. E.; Rebours, B.; Euzen, P.; Toulhoat, H. *J. Phys. Chem. B* **2001**, *105*, 5121.
(7) Nedez, C.; Ray, J.-L. *Environmental Catalysys*; Centi, G., Cristiani, S., Perathoner, S., Forzatti, P., Ed.; EFCE Publications-Series 112; Societa Chimica Italiana: Rome, Italy, 1995; pp 37−40.
(8) Taylor, K. C: *Catal. Rev.−Sci. Eng.* **1993**, *35*, 457.
(9) Knözinger, H.; Ratnasamy, P. *Catal. Rev.−Sci. Eng.* **1978**, *17*, 31.
(10) Shi, B.; Davis, B. H. *J. Catal.* **1995**, *157*, 359
(11) (a) Ozin, G. A. *Chem. Commun.* **2000**, 419. (b) Dabbs, D. M.; Aksay, A. *Annu. Rev. Phys. Chem.* **2000**, *51*, 601. (c) Sánchez, C.; Soler-Illia G. J. de A. A.; Ribot, F.; Lalot, T.; Mayer, C. R.; Cabuil, V. *Chem. Mater.* **2001**, *13*, 3061
(12) Ono, Y.; Kanekiyo, Y.; Inoue, K.; Hojo, J.; Nango, M.; Shinkai, S. *Chem. Lett.* **1999**, 475.
(13) Oishi, G K.; Ishi-i, T.; Sano, M.; Shinkai, S. *Chem. Lett* **1999**, 1089.
(14) Ono, Y.; Nakashima, K.; Sano, M.; Hojo, J.; Shinkai, S. C*hem. Lett.* **1999**, 1119.
(15) Kobyashi, S.; Hanabusa, K.; Susuki, M.; Kimura, M.; Shirai, H. *Chem. Lett.* **1999**, 1077.
(16) Kobyashi, S.; Hanabusa, K.; Hamasaki, N.; Kimura, M.; Shirai, H. *Chem. Mater.* **2000**, *12*, 1523.

10.1021/cm021247t CCC: $22.00
Published on Web 12/16/2002

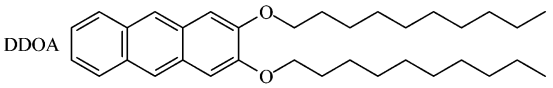

Figure 1. Molecular structure of DDOA (2,3-bis-*n*-decyloxyanthracene).

Indeed, organogelators are low-weight organic molecules capable to form, at very low concentrations (ca. 10^{-3} mol dm^{-3}, less than 1% w/w) in a variety of solvents, thermoreversible physical gels exhibiting strongly anisotropic structures, mostly in the shape of fibers, but also as ribbons, platelets, or cylinders.[21−24] Several families of organogelators such as aliphatic amide derivatives, saccharides, steroids, phthalocyanines, or 2,3-bis-*n*-decyloxyanthracene (DDOA) exist.[25−28] They have been mostly classified according to the main forces occurring at the supramolecular level (H-bonding, van der Waals forces, dipole−dipole interactions, charge transfer, electrostatic interactions, coordination bonds, etc.) and being responsible for the organized stacking of the molecules into the gel phase.

Using the organogelator approach, silica fibers and other siliceous materials presenting novel morphologies and textures have been synthesized by changing the nature of the organogelator: (i) hollow silica tubes presenting a "wrapped" aspect (similar to the lamellar-like pattern observed in spiculae); [19] (ii) tubular silicas presenting a rolled paperlike structure; [19,20] (iii) helical silica or hybrid fibers with chiral information transcribed by selecting templates with the adequate (*R* or *S*) configuration;[17] (iv) using DDOA and DAP organogelators as templates, silica fibers having a double-scale porosity can also be obtained.[29]

These first results are indeed encouraging, as they strongly suggest that the use of organogelators as "templates" will make possible the elaboration of novel materials presenting complex and unique architectures exhibiting multiscale texturing with possible size scales ranging from the nanometer to a fraction of a millimeter.

In this work, an anthracenic organogelator, DDOA (see Figure 1), has been employed as a structure-directing agent to orient the condensation of alumina in the form of fibers. The reproducible production of high-surface, alumina-based fibers (amorphous or crystalline γ-Al_2O_3) exhibiting a bimodal porosity (at the meso- and macroscales) would be of great interest for catalytic applications (higher activity due to the smaller mesopores, and enhanced accessibility due to the presence of macropores), and in general, for all those applications where it is necessary to have an adequate control of host−guest interactions[30,31] and shape selectivity.[32]

Table 1. Conditions for Samples Preparation (Molar Ratios, DDOA Concentration, Catalyst, and pH)

sample	Al:EtOH:H_2O	DDOA final concentration	catalyst (basic)	pH[a]
1	1:20:5	10^{-2} M		<1
2	1:20:5	10^{-2} M	$(CH_3CH_2)_3N$ (TEA)	ca. 2
3	1:20:5	10^{-2} M	NH_3	4−5
B1	1:20:5			<1
B2	1:20:5		$(CH_3CH_2)_3N$ (TEA)	ca. 2

[a] Approximate pH of the overall $AlCl_3$/EtOH/H_2O/(DDOA/base) solution at 70 °C just before organogelation.

2. Experimental Section

2.1. Samples Preparation. The following precursors or products were used: DDOA (synthesized following the procedure described in the literature[33]), $AlCl_3$ (Prolabo, 98%), EtOH (analysis quality, Prolabo, 99.85%), $(CH_3CH_2)_3N$ (TEA, Lancaster Synthesis 99%), and NH_3 (Normapur, 20%). Different alumina-organogelator hybrid samples were prepared by the hydrolysis−condensation of $AlCl_3$ dissolved in an aqueous-ethanolic media containing the organogelator (DDOA) as template (see Table 1). Kinetics of the hydrolysis and condensation reactions of Al^{3+} species were tuned by the addition of a basic catalyst (NH_3 or TEA).

For the preparation of sample **1**, a solution containing $AlCl_3$:EtOH:H_2O in a 1:12:5 molar ratio (first cooled in a glass bath and then heated at 70 °C for 30 min) was added to a 70 °C heated solution of a given amount of DDOA in EtOH. The final $AlCl_3$:EtOH:H_2O molar ratio was equal to 1:20:5, and the final DDOA concentration was 10^{-2} mol L^{-1}. The mixture was then left homogenizing at 70 °C for 45 min, obtaining an acidic transparent solution (pH < 1). Organogelation of DDOA was then performed by removing the sample from heating to let the mixture cool freely at room temperature; a homogeneous organic gel was obtained around 55−60 °C.

In sample **2** the final Al:EtOH:H_2O stoichiometry was the same, but the pH was slightly increased (pH around 2) by adding 1 mol of TEA/mol of $AlCl_3$. The same procedure was used as before, but fractionating the total amount of EtOH (20 mol/Al) to dissolve separately the DDOA, the $AlCl_3$+H_2O mixture and the base. The $AlCl_3$:EtOH:H_2O (1:11:5) acid solution was added to the hot solution of DDOA dissolved in 6 mol of EtOH/Al. After 1 h at 70 °C, the TEA/EtOH mixture (containing 1:3 mol/Al) was added in small portions under vigorous agitation, obtaining a transparent solution in less than 2 h (final pH around 2). A homogeneous organic gel was also obtained by cooling the mixture to room temperature. Sample **3** was prepared similarly to sample **1**, but this time to the acid transparent solution obtained after 45 min at 70 °C was added dropwise an aqueous ammonia solution (10 wt %) up to a pH of ca. 4−5. The highly viscous solution was then cooled to induce organogelation. Two reference samples (**B1** and **B2**) also were prepared without the addition of organogelator, following the same synthetic procedure as with samples **1** and **2**, respectively.

(17) (a) Jung, J. H.; Ono, Y.; Hanabusa, K.; Shinkai, S. *J. Am. Chem. Soc.* **2000**, *122*, 5008. (b) Moreau, J. J. E.; Vellutini, L.; Wong Chi Man, M.; Bied, C. *J. Am. Chem. Soc.* **2001**, *123*, 1509.
(18) Jung, J. H.; Ono, Y.; Shinkai, S. *Angew. Chem., Int. Ed.* **2000**, *39*, 1862.
(19) Jung, J. H.; Ono, Y.; Shinkai, S. *Langmuir* **2000**, *16*, 1643.
(20) Jung, J. H.; Ono, Y.; Shinkai, S. *J. Chem. Soc., Perkin Trans. 2* **1999**, 1289.
(21) van Esch, J. H.; Feringa, B. L. *Angew. Chem., Int. Ed.* **2000**, 39, 2263.
(22) Terech, P.; Furman, I.; Weiss, R. G.; Bouas-Laurent, H.; Desvergne, J. P.; Ramasseul, R. *Faraday Discuss.* **1995**, *101*, 345.
(23) Scartazzini, R.; Luisi, P. L. *J. Phys. Chem.* **1988**, *92*, 829.
(24) Wang, R.; Geiger, C.; Chen, L.; Swanson, B.; Witten, D. G. *J. Am. Chem. Soc.* **2000**, *122*, 2399.
(25) Terech, P.; Weiss, R. G. *Chem. Rev.* **1997**, *97*, 3133.
(26) Abdallah, D.; Weiss, R. G.; *Adv. Mater.* **2000**, *17*, 1237.
(27) Amaike, M.; Kobayashi, H.; Shinkai, S. *Bull. Chem. Soc. Jpn.* **2000**, *73*, 2553
(28) Nakano, K.; Hishikawa, Y.; Sada, K.; Miyata, M.; Hanabusa, K. *Chem. Lett.* (Chemical Society of Japan) **2000**, 1170.
(29) Clavier, G.; Pozzo, J. L.; Bouas-Laurent, H.; Lière, C.; Roux, C.; Sanchez, C. *J. Mater. Chem.* **2000**, *10*, 1725.
(30) Wu, C. G.; Bein, T. *Science* **1994**, *264*, 1757.
(31) Den Exter, M. J.; Jansen, J.C.; van de Graaf, J. M.; Kapteijn, F.; Moulijn, J. A.; van Bekkum, H. *Recent Advances and New Horizons in Zeolite Science and Technology*; Chon, H., Ed.; Studies in Surface Science and Catalysis 102; Elsevier: New York, 1996.
(32) Jones, C. W.; Tsuji, K.; Davis, M. E. *Nature* **1998**, *393*, 52.
(33) Brotin, T.; Untermöhlen, R.; Fages, F.; Bouas-laurent, H.; Desvergne, J. P. *Chem. Commun.* **1991**, 416.

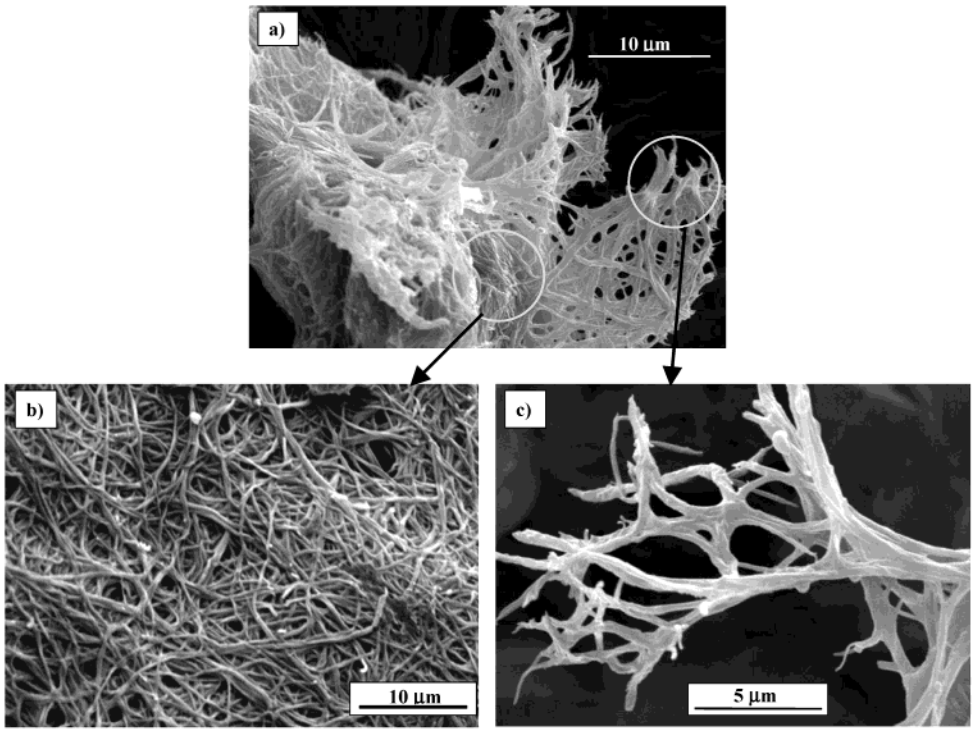

Figure 2. SEM details of hybrid sample **1** before calcination.

Samples were dried in mild conditions by heating at 40 °C for 5 weeks (only 8 days in the case of sample **3**, due to its much faster condensation). A further drying at 100 °C for 3 h was then carried out to better reinforce the condensing inorganic network before the removal of the organogelator.

2.2. Characterization Techniques. Thermal analysis (DSC-TG) of samples was performed with a SDT 2960 Simultaneous DSC-TGA analyzer of TA instruments (20−1000 °C, 5 °C/min). Removal of DDOA after calcination was confirmed by FTIR spectroscopy and also by EDAX and by elemental analysis techniques (performed at CNRS Central Analysis Service, Lyon).

A scanning electron microscope (STEREOSCAN 120 Cambridge Co.) was employed for the observation of noncalcined and calcined powders. Samples were examined as grain mounts following conventional preparation and imaging techniques. The calcined alumina morphologies were also analyzed using transmission electronic microscopy (TEM). The calcined material was embedded within an EPON 812 resin polymerized at 60 °C over 24 h. After microtomic cutting, ultrathin sections, ca. 80−100 nm thick, were observed on a transmission electron microscope (JEOL 100CX II).

The porous structure of 350 °C calcined samples was characterized by the nitrogen adsorption−desorption method at liquid nitrogen temperature using an ASAP 2010 (Micrometrics Co.) analyzer. Calcined samples were degassed in vacuo at 150 °C for 12 h, prior to each measurement. Pore size distributions were determined by the BJH method[34] for mesopores. Specific surface areas were obtained by using the BET equation between 0.05 and 0.30 relative pressures.[35] Total pore volumes (V_t) were determined by the adsorption of nitrogen at a 0.995 relative pressure. In addition, the total surface area S_t, external surface area S_{ex} (including the macropores and secondary mesopores surfaces), micropore volume V_{mi} and primary mesopore volume V_{pm} were calculated using the α_s-plot method[36−38] with a macroporous alumina reference (S_{BET} = 26 m^2 g^{-1} and the amount adsorbed at the relative pressure of 0.4 = 9.82 cm^3 STP g^{-1}).

XRD of calcined samples was carried out by the conventional powder method using a Philips PW1830 diffractometer. FTIR spectroscopy was performed (on KBr pellets) with a Nicolet Magna-IR 550 spectrometer. Raman spectroscopy was recorded using an Yvon U1000 Jobin spectrometer. A more detailed insight of the local chemical structure of the 350 °C calcined materials was obtained by means of the ^{27}Al solid-state NMR. All nuclear magnetic resonance (NMR) spectra were recorded on a MSL 300 Bruker spectrometer. (Spinning frequency: 12 kHz. Pulse: 1 μm. Recycle delay: 1 s.)

3. Results and Discussion

3.1. SEM Characterization of Noncalcined Hybrid Samples. By SEM characterization, dried hybrid sample **1** (prepared in the most acidic conditions, pH < 1) was found to be constituted of a mesh of highly intertwined fibers (see details in Figure 2a−c) around 150−300 nm thick (Figure 2b), and several tens of microns long, which were mostly aggregated conforming highly interconnected fibrous bundles 1−2 μm thick (Figure 2c).

In the case of hybrid sample **2**, in which a controlled amount of triethylamine was added with the aim to trigger alumina condensation reactions, the transcription of the DDOA fibrous structure into the condensing alumina also took place satisfactorily (see Figure 3a), being formed considerably thicker hybrid fibers (300−500 nm thick); remarkably, in this sample the fibers presented a more organized distribution, conforming bundles or lamellae of highly coaligned fibers, which in turn were randomly distributed throughout the hybrid material. A similar co-alignment effect has been described in the literature in the templating of silica fibers

(34) Barret, E. P.; Joyner, L. G.; Halenda, P. H. *J. Am. Chem. Soc.* **1951**, *73*, 373.
(35) Brunauer, S.; Emmet, P. H.; Teller, E. *J. Am. Chem. Soc.* **1938**, *60*, 309.
(36) Gregg, S. J.; Sing, K. S. W. *Adsorption, Surface Area and Porosity*; Academic Press: London, 1982.
(37) Kaneko, K.; Ishii, C.; Ruike, M.; Kuwabara, H. *Carbon* **1992**, *30*, 1075.
(38) Kruk, M.; Jaroniec, M. *Langmuir* **1997**, *13*, 6267.

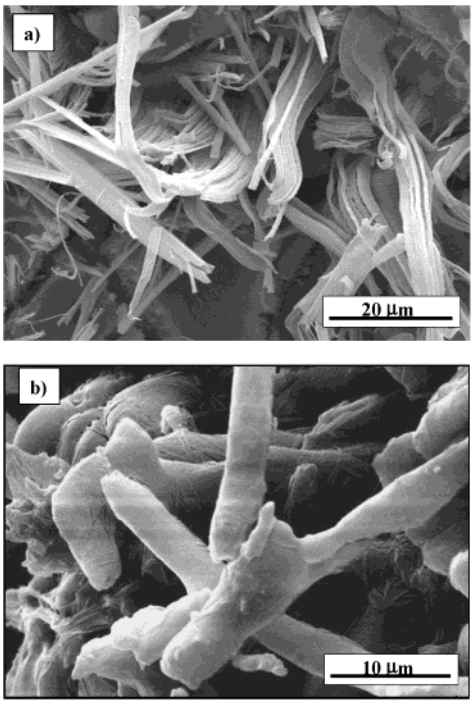

Figure 3. SEM details of hybrid samples **2** (a) and **3** (b) before calcination.

by DDOA.[29] Thus, the slight increase of pH in sample **2** (pH ca. 2) by adding the organic base (TEA) proves to have an important effect: addition of the base would effectively trigger the formation and growth of the alumina inorganic network by accelerating condensation reactions; this fact not only results in thicker fibers but also seems to induce the coalignment of the fibers.

Therefore, SEM characterization confirmed the efficient transcription of the DDOA fibrous structure during alumina condensation, when organogelation was processed prior to the formation of the inorganic gel (samples **1** and **2**). Thus, condensation by thermal aging of the Al^{3+} complex species present in the acidic ethanolic solution was compatible with the presence of the DDOA fibrils, and the successful templating of the fibrous network suggests the existence of an adsorption driving force that makes the propagating alumina species further condense onto the DDOA fibers surface. However, the type of interactions between alumina condensing oligomers and DDOA organogel is still not well-understood: electrostatic and/or hydrogen-bond interactions could play an important role in the transcription process, similarly to what has been suggested for silica fibers templated by DDOA[29] or by cationic-charged gelators.[39] This seems a probable mechanism but the possibility that the fibrous structures originate from replication of the phase separated solvent (that is, not only on but also between the filaments to give an inverse replica) cannot be ruled out.

In contrast, sample **3** was observed to be eminently granular, with only a minor presence of fibers (see Figure 3b), considerably thicker (several micrometers thick) than those observed in previous samples. The surface of these fibers was covered by much thinner fibrils, possibly corresponding to the gelator. In this sample, the pH was increased with diluted NH_3 up to 4−5, and therefore condensation of alumina species was still much faster than in sample **2**, proceeding randomly before the formation of the organic gel. Consequently, replication of the gelator fibers could not satisfactorily be accomplished, since bulk polymerization of the alumina took place prior to the formation of the fibrous organic assemblies, mainly resulting in the conventional granular structure.

In conclusion, the results obtained confirm that hybrid DDOA-alumina gel fibers can be obtained using DDOA gelator fibers as a template, with an appropriate control of the kinetics of condensation of alumina species: at a pH below ca. 2−3 (samples **1** and **2**), the fibrous network conformed by the organogel can be satisfactorily transcribed into the condensing Al^{3+} complexes, but if the pH is further increased (sample **3**), the conventional bulk condensation prevents an efficient templating of DDOA fibers. In addition, fibers thickness and aggregation have shown to be very sensitive to pH conditions: a remarkable thickening and co-alignment effect of the otherwise highly intertwined hybrid fibers was induced by the addition of a controlled amount of triethylamine. Further experimentation should be conducted to find a possible mechanism or explanation for such behavior, which is out of the scope of the present work.

3.2. Thermal Analysis and Elimination of Organogelator. Thermal analysis characterization of the organogelator and of 100 °C dried samples was carried out before proceeding to the calcination of the samples. According to the DSC-TG curves shown in Figure 4a, the organogelator (DDOA) decomposes in different steps from 250 °C, the main weight losses (with associated exothermic peaks) occurring between 250 and 350 °C (63%) and between 350 and 550 °C (25%). In the case of sample **1** (see DSC-TG curve in Figure 4b), a single and intense endothermic peak is observed at 150 °C, with a high weight loss associated (around 70−75%) between 100 and 200 °C. This weight loss cannot be attributed to DDOA decomposition, since by EDAX analysis this sample dried at 100 °C was shown to contain only traces of C (see Table 2). Considering the low DDOA wt % present in dried hybrid samples (2−2.5 wt %), DDOA removal is almost inappreciable by DSC-TG analysis. Accordingly, this endothermic peak could be mainly attributed to the removal of chlorides and of hydration water and adsorbed ethanol. Then, a weak and broad exothermic band between 200 and 700 °C may be observed (10 wt % loss between 200 and 500 °C, and only a 1 wt % loss between 500 and 700 °C); in this region, different processes would be occurring with an associated weight-loss: complete removal of chlorides, organogelator decomposition, and further condensation of hydroxyl groups. Only at temperatures so high as 750 °C an exothermic region begins, suggesting that the condensing alumina remains amorphous up to such temperatures, at which structural reorganizations giving rise to the progressive crystallization of the series of transition aluminas (γ-$Al_2O_3 \rightarrow \delta$-$Al_2O_3 \rightarrow \theta$-$Al_2O_3 \rightarrow \alpha$-$Al_2O_3$)[4−6] would start occurring.

The DSC-TG curves of sample **2** (see Figure 4c) present some slight differences with respect to sample **1**. Effectively, two endothermic peaks may be observed

(39) Ono, Y.; Nakashima, K.; Sano, M.; Hojo, J.; Shinkai, S. *J. Mater. Chem.* **2001**, *11*, 2412.

Table 2. Al/O/C/Cl mol % Ratios Obtained by EDAX Semiquantitative Analysis of Samples 1 and 2: As-Prepared (100 °C Dried), after Intermediate Calcines (125 and 205 °C), and after the Final Calcine at 350 °C[a]

S[b]	dried sample (100 °C/3 h)	calcined sample (125 °C/2 h)	calcined sample (205 °C/2 h)	350 °C calcined final materials	350 °C calcined final materials (chemical analysis)
1	8/69/*c*/23	20/70/*c*/10	29/68/*c*/3	32/67/*c*/1	27.8/47.5/1.5/0.9/22.3
2	4/36/50/10	5/38/51/6	16/66/15/2	28/72/*c*/0	23.8/41.9/1.0/0.1/33.2

[a] Last column shows the Al/O/C/Cl/H mol % ratios of final materials obtained by quantitative chemical analysis techniques. [b] S = sample. [c] C was present in a small percentage below 2σ (σ: standard deviation).

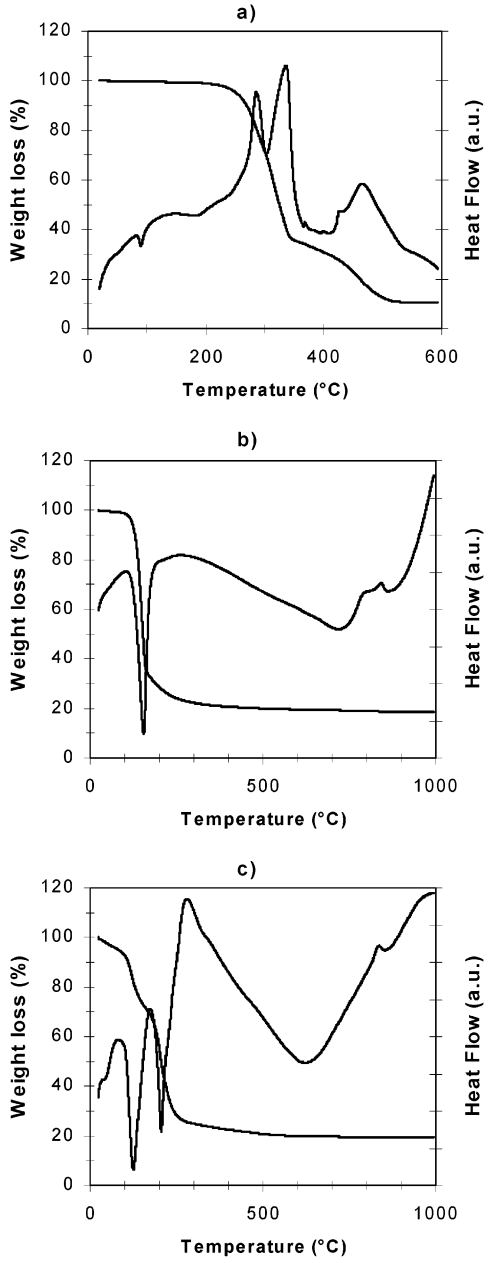

Figure 4. Thermal analysis curves (DSC-TG) of DDOA (a), and of samples **1** (b) and **2** (c).

at 125 °C and at 205 °C, followed by an intense exothermic peak around 280 °C, with associated weight-losses of 26% (20−150 °C), 45% (150−250 °C), and 9% (250−600 °C), respectively. Semiquantitative EDAX analysis of hybrid samples heat treated at 125 and 205 °C (see approximate Al:O:C:Cl molar ratios in Table 2), confirmed that almost all chlorides are removed between 100 and 200 °C in both samples, and that organics removal occurs above 150 °C in sample **2**; accordingly, the first endothermic peak at 125 °C would be associated to the partial removal of chlorides (and of hydration water), while the second endothermic peak at 205 °C could correspond to the partial volatilization of the $(CH_3CH_2)_3NH^+Cl^-$ species resulting from the neutralization of HCl (formed in the $AlCl_3$ hydrolysis) by the added TEA; this salt decomposes at 260 °C and would be responsible for the intense exothermic band around 280 °C, which would be masking the DDOA decomposition. The exothermic region associated to the crystallization of transition aluminas may be seen to start in this sample at slightly lower temperatures (around 650 °C), suggesting that condensation reactions were slightly faster in this sample, as expected.

According to thermal analysis results, hybrid samples **1** and **2** were first calcined at 150 °C for 2 h. This treatment allowed us to remove by evaporation the hydration water, adsorbed ethanol and most of chlorides, and at the same time to consolidate the inorganic Al-skeleton before DDOA removal. Then, the pyrolytic decomposition of organogelator fibers was promoted with a first calcination at 350 °C (2 h under Ar flow and 4 h under air); finally, a further calcination at 350 °C for 4 h under air was carried out to ensure the complete removal of residual C and of entrapped chlorides, and to further condense the alumina-based network (eminently amorphous at this low temperature).

Removal of DDOA after calcination was confirmed by FTIR spectroscopy (discussed later), by EDAX semiquantitative analysis, and also by quantitative chemical analysis performed on the final 350 °C calcined samples (see also Table 2). As may be appreciated in Table 2, both samples were practically free of C and of Cl (C, <1.5 mol %, and Cl, <0.9−1 mol %). As a relevant point, analysis data showed that the final compounds were still considerably hydrated (O:Al:H molar ratios equal to 2:1.2:0.9 and 2:1.1:1.6 in samples **1** and **2**, respectively), and the stoichiometry of the obtained amorphous aluminas was close to that of Al oxyhydroxydes (for instance, the O:Al:H ratio is 2:1:1 for AlO(OH)).

3.3. Preservation of Fibrous Assemblies after Calcination. Representative SEM details of samples **1** and **2** after calcination at 350 °C are shown in Figure 5. These observations evidenced that the fibrous assemblies constituting the hybrid materials were highly preserved after removal of the organic imprint by calcination. In effect, sample **1** (see Figure 5a−d) was mostly constituted by a mesh of intertwined fibers (around 200−300 nm thick) considerably aggregated forming fibrous bundles or platelike assemblies, as a result of the partial condensation of alumina in the interfibrilar voids. Regarding sample **2**, highly coaligned fibers (200−500 nm thick) conforming randomly dispersed fibrous lamellae were perfectly conserved after

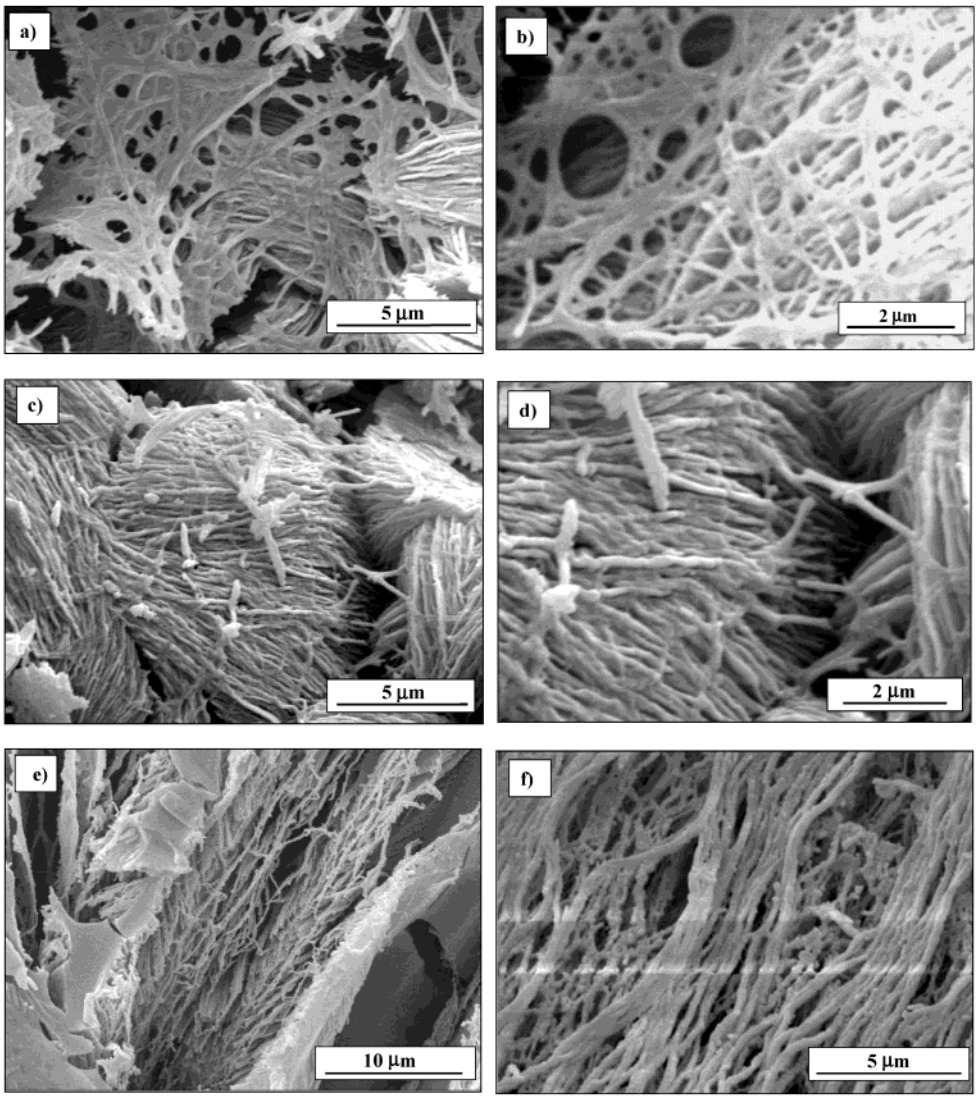

Figure 5. SEM details of alumina-based samples **1** (a−d) and **2** (e and f) calcined at 350 °C.

calcination. In contrast, reference samples (**B1** and **B2**) prepared without the addition of DDOA exhibited lamellar or platelet morphology after calcination, which is commonly found in aluminum oxyhydroxides.[40]

TEM characterization of calcined samples **1** and **2** confirmed in both cases the anisotropic distribution of the fibrous assemblies at the macroscale, due to the presence of highly intertwined fibers or bundles (specially in sample **1**), but at the mesoscopic level, the presence of partially aligned, very thin and elongated porous channels (a few nanometers thick) was clearly observed (see representative TEM detail of sample **1** in Figure 6). Related to this, TEM characterization let us appreciate much thinner fibrils (15−30 nm) than those previously observed by SEM characterization; this result would be in accordance with previous reports suggesting that DDOA fibers and/or fibrous bundles (50−150 nm-thick) are rather formed by the aggregation of much thinner fibrils (ca. 10 nm).[29]

Very interestingly, the samples also were calcined at higher temperatures (500 °C and 800 °C; 6 h under air), where crystallization occurs according to the previous thermal analysis data, and the fibrous morphology still was preserved. Some SEM details corresponding to sample **1** after calcination at 800 °C may be seen in Figure 7.

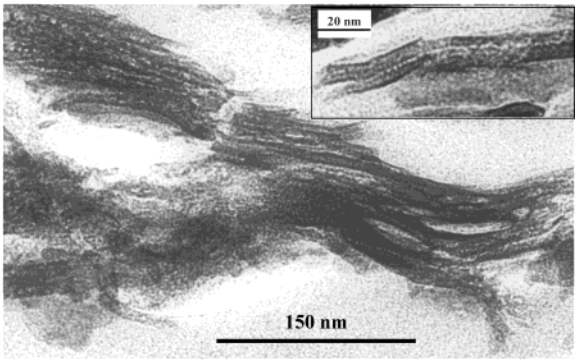

Figure 6. TEM micrographs (microtomic cuts) at different magnifications of alumina-based sample **1** calcined at 350 °C.

In conclusion, we have seen that DDOA can be successfully used to template the condensation of alumina species in the form of fibers; moreover, the preparation conditions here used let us obtain a partially condensed fibrous alumina with the sufficient strength or consistency to withstand the calcination

(40) Trebillon, E. (Rhône-Poulenc specialités chimiques) French Patent 2 520 722, **1982**.

Table 3. Structural Parameters for Samples Calcined at 350 °C

sample	BET specific surface area S_{BET} (m^2/g)	total surface area S_t (m^2/g)	external surface area S_{ex} (m^2/g)	primary mesopore surface area S_{pm} (m^2/g)	total pore volume V_t (cm^3/g)	primary mesopore volume V_{pm} (cm^3/g)	BJH average diameter D_{BJH} (nm)	primary mesopore diameter D_{pm} (nm)
1	159	152[a]	25	127	0.40	0.271[b]	10	8.5[c]
B1	192	186[a]	9	177	0.60	0.538[b]	11	12.1[c]
2	299	296	7	289	0.28	0.250	4	2.9[c]
B2	355	350	4	346	0.41	0.390	4	4.5[c]

[a] The α_s-plots for these samples indicated the presence of some microporosity (the micropore volume V_{mi} is equal to ca. 0.0037 and 0.0025 cm^3/g for the samples **1** and **B1**, respectively), so the total surface area provides the surface area of meso and macropores excluding the surface area of micropores. [b] Correction for the micropore volume was introduced. [c] The primary mesopore diameter D_{pm} was calculated from the primary mesopore surface area and primary mesopore volume: $D_{pm} = 4V_{pm}/S_{pm}$.

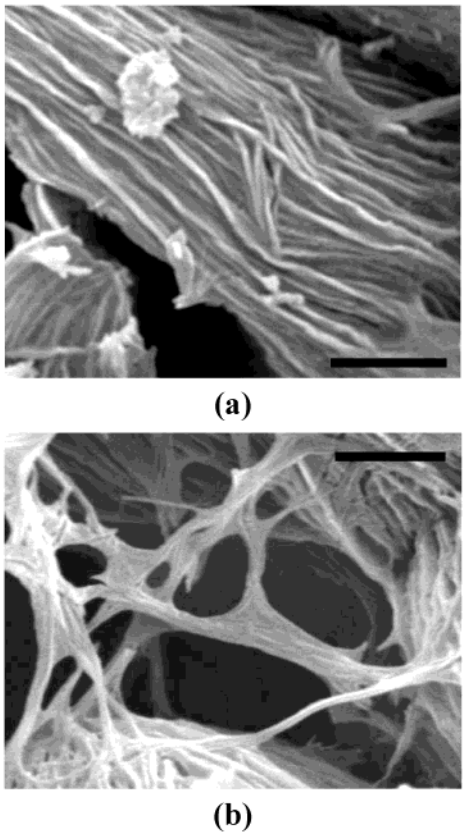

Figure 7. SEM details (bar length = 2 μm) of alumina-based sample **1** after calcination at 800 °C (6 h/air); XRD correspond to α-Al_2O_3 + residual transition aluminas (see also Figures S3 and S4 in Supporting Information).

treatment without disruption of the fibrous structure, even after crystallization of transition aluminas and of α-Al_2O_3 (see Supporting Information).

3.4. Characterization of the Porous Structure. Characterization of the porosity of 350 °C calcined samples (see Table 3 and Figures 8 and 9) evidenced remarkable differences in the porous structure depending on the preparation conditions (pH-catalyst) and also arising from the use of DDOA fibrils as a template. As may be seen, the BET specific surface areas of the calcined aluminas were all relatively high (160−355 m^2/g), improving in some cases (**2** and **B2** samples) the values reported in the literature for amorphous and transition γ-aluminas (180−240 m^2/g).[41] In all cases, the isotherms corresponded to the type IV in the Brunauer classification, which is associated to mesoporous materials. In addition, all the samples were almost free of microporosity (the V_{mi} was always below 3−4%), and consequently, the obtained calcined aluminas may be considered to present in all cases a bimodal porosity, at the meso and macro scales (the later being indirectly confirmed by the measured external surface, and also observed by SEM).

As a previous consideration, irrespective of the addition of DDOA as a template, the samples prepared at a pH around 2 by adding TEA (**2** and **B2**) exhibited much higher surface areas than the most acidic samples (**1** and **B1**), suggesting an important effect of preparation conditions on the porosity. This effect was analyzed in more detail by comparing the isotherms, BJH curves, and α_s-plot representations of reference samples **B1** and **B2** (Figures 8b and 9b, respectively). The form of the hysteresis loops was quite similar in both samples, corresponding to the standard type H2 (on the left) and a capillary condensation phenomena occurred in these pores (according to the α_s-plot representation on the right). Therefore, both samples would be constituted by polydispersed aggregate particles originating "ink-bottle" shaped primary mesopores. Despite of this similarity of pore forms, the hysteresis cycle may be seen to start at considerably lower relative pressures in **B2** sample than in **B1** sample (0.42 vs 0.5), indicating the presence of smaller pores in the former; moreover, the hysteresis loop in **B1** is still not completely saturated at relative pressures close to 1, suggesting a higher presence of secondary mesopores and/or macropores in this sample (probably resulting from the polydispersion of the primary-mesoporous aggregates). The BJH curves also confirmed the higher uniformity of pore sizes and the smaller pore sizes in **B2** with respect to **B1**. The total surface areas (S_{pm}) and primary mesopore volumes (V_{pm}) calculated by the α_s-plot method were very close in both samples to the respective BET surface areas and total pore volumes (see Table 3). This result confirms that the whole porosity in both reference samples is due to primary mesopores.

As it was to be expected, the employment of DDOA as a template also produced remarkable differences at the mesoscopic level, apart from the evident effect on the macroscopic morphology derived from the successful fibers transcription. In the case of sample **1** (see Figure 8a), the isotherm curve presented an hysteresis loop composed of two different regions: the first hysteresis region at low relative pressures (starting from 0.42 to 0.45 and up to 0.85) was of the standard H2 form associated to capillary condensation phenomena as in the reference **B1**, also indicating the presence of ink-

(41) Franck, J. P.; Martino, G. *Progress in Catalyst Deactivation*; Figuereido, J. L., Eds.; Martinus Nijhoff Publishers: The Hague, 1982; p 355.

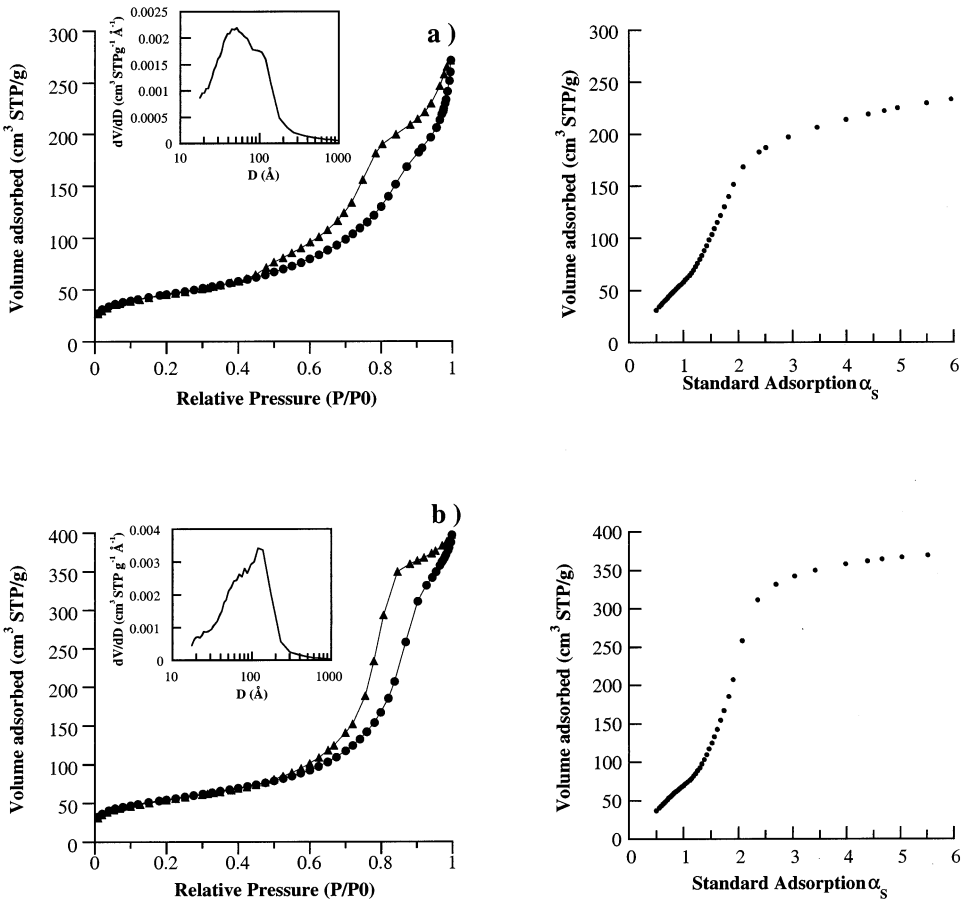

Figure 8. Typical N_2 isotherms (● adsorption, ▲ desorption) and BJH distribution curves (left), and $V_{adsorbed}$ vs α_s-plot representations (right) of alumina-based samples **1** (a) and **B1** (b) calcined at 350 °C.

bottle shaped mesopores. In contrast, the second hysteresis region was not saturated at relative pressures close to 1 and was of the standard H3 form. Effectively, the S_{pm} and V_{pm} values calculated from the α_s-plot representation were lower than the values of BET surface area and total pore volume. Accordingly, porosity in this sample is not only due to primary mesopores, but there is also a nonneglectable contribution of secondary mesopores and macropores, as confirmed by the much higher external surface (25 m^2 g^{-1}). In addition, the first hysteresis associated to primary ink-bottle mesopores starts at relative pressures (0.42−0.45) considerably lower than those used for the reference **B1** (0.5). This fact is indicating that the size of primary mesopores is slightly lower in this sample than in the reference, as it may be appreciated in the BJH curves, and as it also may be confirmed by the lower average size of primary mesopores calculated by the ($4V_{pm}/S_{pm}$) method using the α_s-plot V_{pm} and S_{pm} values (10 vs 11 nm). As a relevant point, the size of these smaller primary mesopores (with sizes around 4−10 nm) correlates quite well with the size of the channel-like elongated mesopores arising from DDOA removal, which had been previously observed in this sample by TEM characterization (Figure 6). Therefore, the results obtained in this sample are in agreement with the successful texturation of the amorphous alumina as highly intertwined hollow fibers. Removal of DDOA fibrils (around 10 nm thick, aggregated in bundles 50−150 nm thick) would be responsible for the generation of very small channel-like primary mesopores (4−10 nm), and the aggregation of the fibrils in fibrous bundles and/or lamellae (highly intertwined) would be generating mesopores of higher sizes responsible for the second hysteresis region at higher relative pressures.

In the case of sample **2**, however, the hysteresis loop had the H4 standard form (Figure 9a, left), and also was associated to capillary condensation phenomena by comparison with the αs-plot representation (right). According to recent observations,[42,43] hysteresis loops of the type H4, usually associated to platelike particles forming narrow slitlike pores, may merely arise from the presence of large mesopores embedded in a matrix with pores of much smaller size. Therefore, the presence in sample **2** of aggregated lamellae conformed by coaligned and/or intertwined hollow fibers (as observed by SEM) would be consistent with this model: the aggregated fibrous lamellae would be constituted by interfibrilar large mesopores or macropores (larger than in sample **1**, since they are not detected in the BET isotherms), along with smaller mesopores (around 3 nm, according to BJH curve, and also in accordance to the $4V_{pm}/S_{pm}$ value from the α_s-plot representation) probably arising from DDOA removal, though primary mesopores of the reference sample (**B2**, Figure 8b) also presented similar sizes (4−5 nm).

3.5. Chemical Characterization of Calcined Materials. XRD characterization evidenced the amorphous

(42) Kooyman, P. J.; Verhoef, M. J.; Prouzet, E. *Stud. Surf. Sci. Catal.* **2000**, *129*, 535.
(43) Kruk, M.; Jaroniec, M. *Chem. Mater.* **2001**, *13*, 3169.

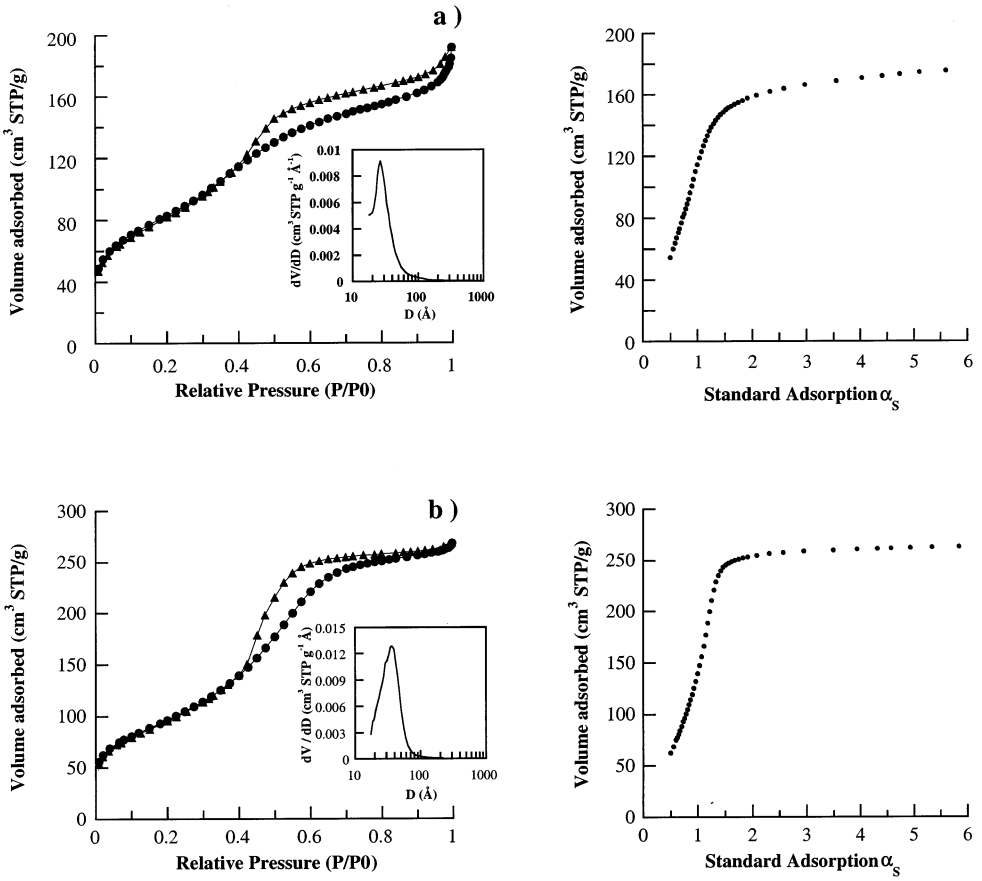

Figure 9. Typical N_2 isotherms (● adsorption, ▲ desorption) and BJH distribution curves (left), and $V_{adsorbed}$ vs α_s-plot representations (right) of alumina-based samples **2** (a) and **B2** (b) calcined at 350 °C.

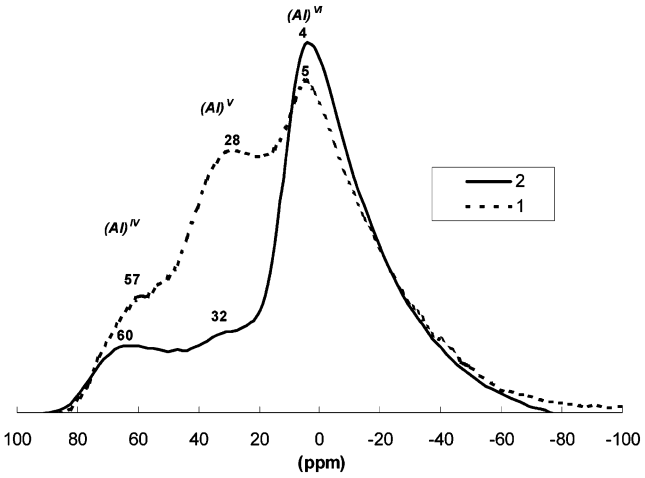

Figure 10. Solid ^{27}Al NMR spectra corresponding to 350 °C-calcined, alumina-based samples **1** and **2**. (Spinning frequency: 12 kHz. Pulse: 1 μm. Recycle delay: 1 s.)

nature of the alumina-based samples after calcination at 350 °C (and even after recalcination at 500 °C/6 h), as expected attending to thermal analysis results. In this respect, crystallization of γ-Al_2O_3 from bohemite precursors has been reported to occur through a topotactic transformation at temperatures between 300 and 500 °C,[6,44] though it can take place even at higher temperatures (as in our case).

The 350 °C calcined, amorphous materials were then analyzed by FTIR−Raman spectroscopic techniques.[45−48] The Raman spectra of the calcined materials did not show well-defined peaks, corroborating the amorphous character of the samples. On the other hand, the IR spectra of samples **1** and **2** confirmed the complete removal of organogelator after calcination (only traces of carbon would be present considering the very weak carboxylate peaks around 1400−1500 cm^{-1}), and showed slight differences in the Al−O stretching region: a broad band extending between 400 and 1000 cm^{-1} was observed in both cases, but in sample **1** this band was more pronounced in the 700−850 cm^{-1} region, while in sample **2** the region between 620 and 700 cm^{-1} was more intense. Several authors have assigned the 550−850 cm^{-1} and the 750−850 cm^{-1} regions to symmetric stretching and bending modes of AlO_6 and AlO_4 vibrations, respectively.[49] Therefore, the IR spectra could be suggesting a higher AlO_6/AlO_4 ratio in sample **2** than that in sample **1**, though other authors[50] have expressed the opinion that the broad band between 400 and 900 cm^{-1} must be rather attributed to a "complex AlO_6 and AlO_4 interactive vibration".[48,50]

To bring some light to the matter, a more detailed insight of the local chemical structure of the 350 °C-

(44) Wolverton, C.; Hass, K. C. *Phys. Rev. B* **2000**, *63*, 024102, 5121.
(45) Morterra, C.; Emanuel, C.; Cerrato, G.; Magnacca, G. *J. Chem. Soc., Faraday Trans.* **2002**, *88*, 339
(46) Mariotto, G.; Cazzanelli, E.; Carturan, G., Maggio di, R.; Scardi, P. *J. Solid State Chem.* **1990,** *86*, 263.
(47) Assih, T.; Ayral, A.; Abenoza, M.; Phalippou, J. *J. Mater. Sci.* **1988**, *23*, 3326.
(48) Fripiat, J. J.; Alvarez, nL. J.; Sánchez, J.; Martínez, E.; Saniger, J. M.; Sánchez, N. *Appl. Catal. A: Gen.* **2001**, *215*, 91.
(49) Colomban, P. H., *J. Mater. Sci.* **1989**, *24*, 3002.
(50) Saniger, J. M.; Sánchez, N. A.; Flores, J. O. *J. Fluorine Chem.* **1998**, *88*, 117.

calcined materials was obtained by means of the ^{27}Al solid NMR technique.[51−53] In Al−O environments, the ^{27}Al shifts for 4-, 5-, and 6-coordinated Al are well separated, occurring at about 50−80, 30−40, and 10−15 ppm,[54,55] respectively. As may be appreciated in Figure 9, the ^{27}Al NMR spectra of both calcined samples presented three signals (partially overlapped) corresponding to 4-, 5-, and 6-coordinated Al (peaks at 57, 28, and 5 ppm in sample **1**, and at 60, 32, and 4 ppm in sample **2**). As a relevant point, the relative intensity (integrated area obtained by deconvolution techniques) of the bands associated to each Al coordination site was considerably different in both samples: the Al^{VI}:Al^{V}:Al^{IV} ratio was 55:35:15 in sample **1** and 73:13:14 in sample **2**. The much higher proportion of octahedrally coordinated Al in sample **2** would be in accordance with the differences observed in the Al−O stretching vibration of the IR spectra.

Hydrated aluminas contain Al exclusively in octahedral positions, similarly to α-Al_2O_3, while in the case of crystalline transition aluminas, Al is located in both tetrahedral and octahedral sites (the Al^{VI} content in spinel-based transition γ-, δ-, and η-aluminas ranges in general between 62.5 and 75%, and decreases to 50% for θ-Al_2O_3).[44,56] Considering these results, the ^{27}Al NMR spectra of the calcined samples are consistent with amorphous aluminas in which the structural reorganization involving the migration of Al cations from pentacoordinated sites toward octahedral and tetrahedral positions (necessary to form the transition alumina) has still not been completed.

Finally, the materials were recalcined at higher temperatures (800 °C), and the crystallization of transition "spinel-based" aluminas (still not present at 500 °C) and of α-Al_2O_3 (well-crystallized, major phase at 800 °C) was clearly confirmed by XRD characterization (the pattern of sample **1** after calcination at 800 °C is shown as Supporting Information). As previously mentioned, the alumina-based materials conserved to a high extent the fibrous morphology even after calcination at 800 °C and crystallization of corundum, confirming again the high efficiency of the templating method here described, and further reinforcing the relevance and versatility of this smart synthetic approach for designing amorphous and/or crystalline fibrous aluminas of great interest for catalytic applications.

Acknowledgment. The authors acknowledge *l'Institut Français du Pétrole* for the financial support of Pidol, L. and particularly Patrick Euzen (IFP) for his interest on this research and for helpful discussions. The authors also thank Maquet, J., for his valuable help in performing the ^{27}Al solid RMN experiments. Llusar, M., is grateful to the European Community Marie Curie Individual Fellowship Program for financial support, and to the Host Center (*Laboratoire de Chimie de la Matière Condensée* of Paris VI University) for enabling the realization of the work.

Supporting Information Available: SEM micrographs of calcined reference samples **B1** and **B2**, IR spectra of 350 °C calcined samples **1** and **2**, SEM micrograph of sample **1** calcined at 800 °C, and XRD pattern of sample **1** calcined at 800 °C (PDF). This material is available free of charge via the Internet http://pubs.acs.org.

CM021247T

(51) Slade, R. C. T.; Southern, J. C.; Thompson, I. M. *J. Mater. Chem*. **1991**, *1*, 875.
(52) Meinhold, R. H.; Slade, R. C. T.; Newman, R. H. *Appl. Magn. Reson*. **1993**, *4*, 121.
(53) Pecharromán, C.; Sobrados, I.; Iglesias, J. E.; González-Carreño, T.; Sanz, J. *J. Phys. Chem. B* **1999**, *103*, 6160.
(54) Mühller, D.; Gessner, W. *Chem. Phys. Lett*. **1981**, *79*, 59.
(55) (a) Akitt, J. W.; Greenwood, N. N., Khandelwal, B. L., Lester, G. D. *J. Chem. Soc., Dalton Trans.* **1972**, 604. (b) Akitt, J. W. Elders, J. M. *J. Chem. Soc., Dalton Trans.* **1988**, 1347.
(56) Zhou, R. S.; Snyder, R. L. *Acta Crystallogr., Sect. B: Struct. Sci*. **1991**, *B47*, 617.